Geophys. J. Int. (2006) **166,** 1148–1160 doi: 10.1111/j.1365-246X.2006.02972.x

Regional tomographic inversion of the amplitude and phase of Rayleigh waves with 2-D sensitivity kernels

Yingjie Yang* and Donald W. Forsyth

Department of Geological Sciences, Brown University, 324 *Brook Street, Providence,* RI 02912, *USA. E-mail: yingjie_yang@brown.edu*

Accepted 2006 February 22. Received 2006 February 21; in original form 2005 June 7

SUMMARY

In this study, we test the adequacy of 2-D sensitivity kernels for fundamental-mode Rayleigh waves based on the single-scattering (Born) approximation to account for the effects of heterogeneous structure on the wavefield in a regional surface wave study. The calculated phase and amplitude data using the 2-D sensitivity kernels are compared to phase and amplitude data obtained from seismic waveforms synthesized by the pseudo-spectral method for plane Rayleigh waves propagating through heterogeneous structure. We find that the kernels can accurately predict the perturbation of the wavefield even when the size of anomaly is larger than one wavelength. The only exception is a systematic bias in the amplitude within the anomaly itself due to a site response.

An inversion method of surface wave tomography based on the sensitivity kernels is developed and applied to synthesized data obtained from a numerical simulation modelling Rayleigh wave propagation over checkerboard structure. By comparing recovered images to input structure, we illustrate that the method can almost completely recover anomalies within an array of stations when the size of the anomalies is larger than or close to one wavelength of the surface waves. Surface wave amplitude contains important information about Earth structure and should be inverted together with phase data in surface wave tomography.

Key words: sensitivity kernels, surface waves, tomography.

GJI Seismology

INTRODUCTION

In traditional surface wave tomography, ray theory is assumed to resolve heterogeneities of lithosphere and upper mantle with the great-circle ray approximation (e.g. Woodhouse & Dziewonski 1984; Trampert & Woodhouse 1995; van der Lee & Nolet 1997) or by tracing rays through a heterogeneous earth model. However, ray theory is only valid when the scale of heterogeneities is much larger than the wavelength and the width of the Fresnel zone. This theoretical limitation calls into question the ability to discover small-scale structure using surface wave tomography based on ray theory even with the fast-growing abundance of seismic data. When the length scale of heterogeneities is comparable to the wavelength, the sensitivity of surface waves to heterogeneous structure off the ray path is significant and finite frequency effects should be taken into account. In recent years, the finite-frequency properties of surface waves have been considered in a number of global surface wave tomography studies (Clevede *et al.* 2000; Spetzler *et al.* 2002; Ritzwoller *et al.* 2002; Yoshizawa & Kennett 2002; Zhou *et al.* 2004).

*Currently at: Center for imaging the Earth's interior, Department of Physics, University of Colarado at Boulder, Boulder, CO 80309-0390, USA, E-mail: yingjie.yang@colorado.edu

However, in regional teleseismic surface wave tomography, the conventional two-station method is still widely used. Phase traveltimes along great-circle paths between many pairs of stations are combined to find 2-D local phase velocities. Surface wave amplitude has not been included in these inversions due to complicated effects such as multipathing, focusing/defocusing and attenuation. In regional tomography, the length scale of structures we are interested in is often comparable to the wavelength or even smaller than the wavelength, which urges us to consider finite frequency effects. To represent the effects of scattering of waves outside the regional array, Forsyth & Li (2004) developed a method that represents an incoming wave with the interference of two plane waves. For each plane wave, a Gaussian sensitivity function was utilized to represent the finite width of the response of surface waves to structure along the ray path. The interference of two plane waves can often represent well the character of non-planar incoming waves caused by multipathing and scattering with far fewer parameters than the more general approach of Friederich and Wielandt (1995), thus providing more stability in the inversion for velocity variations within the array. However, the Gaussian sensitivity function, which assumes the sensitivity is equal along the ray path and decays as a Gaussian function in the direction perpendicular to ray path, does not describe the sensitivity accurately.

In this study, we use the kernels derived by Zhou *et al.* (2004) to represent the sensitivity of surface waves to structure. By comparing

with numerical simulation, we evaluate the accuracy of the sensitivity kernels based on the Born approximation in describing the wavefield variation caused by heterogeneous structure. We develop a regional surface wave tomography method based on the sensitivity kernels and apply the method to synthesized data. Finally, we compare the recovered phase velocity structure with that found from the previous method based on Gaussian sensitivity function.

THEORY OF FINITE-FREQUENCY PROPERTIES OF SURFACE WAVES

In traditional surface wave tomography, ray theory is commonly utilized to interpret relative phase shifts along great circle paths in terms of local relative phase velocities. Propagation of a surface wave on the surface of the Earth is assumed to be along an infinitely thin ray path. Ray theory is valid when the characteristic scale of heterogeneous structure is much larger than the wavelength. However, when the scale of heterogeneous structure is close to the wavelength or even smaller, finite-frequency effects will be significant and ray theory cannot describe the phase shift accurately. In order to resolve finer heterogeneous structure, we have to take finite-frequency effects into account in surface wave tomography. In 2004, Zhou *et al.* derived 3-D sensitivity kernels for surface waves based on single-scattering (Born) approximation on the Earth surface. The sensitivity kernels are formulated in the form of surface wave mode summations for measured phases and amplitudes. For the single-frequency case, phase and amplitude variations, $\delta\phi(\omega)$ and $\delta \ln A(\omega)$, in a perturbed earth model relative to the reference earth model can be expressed as following:

$$\begin{aligned}\delta\phi(\omega) &= \iiint_{\oplus} K_{\phi}^{m}(x,\omega)\delta m(x)\, d^3x, \delta \ln A(\omega) \\ &= \iiint_{\oplus} K_{A}^{m}(x,\omega)\delta m(x)\, d^3x, \end{aligned} \quad (1)$$

where δm is shorthand for $\delta\alpha/\alpha$, $\delta\beta/\beta$, $\delta\rho/\rho$, and $K_{\phi}^{m}(x,\omega)$ and $K_{A}^{m}(x,\omega)$ are the phase and amplitude sensitivity kernels respectively.

Furthermore, they show that by using the forward-scattering approximation and neglecting mode-coupling effects, the 3-D sensitivity kernels, expressing the sensitivities to 3-D perturbations in density, shear wave velocity and compressional wave velocity, can be combined to form 2-D sensitivity kernels expressing the sensitivities to the local phase velocity perturbation, $\delta c/c$. The 2-D sensitivity kernels are defined as:

$$\delta d = \iint_{\Omega} K_{d}^{c}(r,\omega)(\delta c/c)\, dx^2, \quad (2)$$

where the integration is over the Earth's surface. δd is shorthand for the phase delay, $\delta\phi$, or the relative amplitude variation, $\delta \ln A$, with corresponding phase kernel $K_{\phi}^{c}(r,\omega)$ or amplitude kernel $K_{A}^{c}(r,\omega)$.

In regional surface wave array tomography using teleseismic sources, incoming waves are generally regarded as plane waves when propagating through a study region with maximum dimensions of hundreds of kilometres. The sensitivity kernels for a plane wave can be simplified as,

$$K_{\phi}^{c}(r,\omega) = \mathrm{Im}\left(\frac{k^2 R'' e^{-i[kx''-k\Delta x+\pi/4]}}{R\sqrt{2\pi k x''}}\right), \quad (3)$$

and

$$K_{A}^{c}(r,\omega) = -\mathrm{Re}\left(\frac{k^2 R'' e^{-i[kx''-k\Delta x+\pi/4]}}{R\sqrt{2\pi k x''}}\right), \quad (4)$$

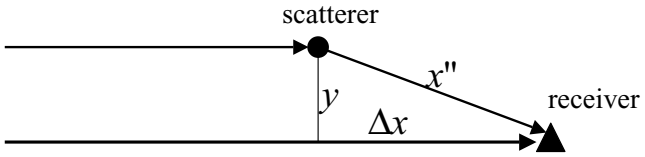

Figure 1. The schematic figure of single scattering for a plane surface wave propagating from left to right. x'' is the scatter-receiver distance; y is the perpendicular distance from the scatterer to the direct incoming ray recorded by the receiver; Δx is the differential propagating distance between the direct incoming wave arrived at the receiver and that arrived at the scatterer.

where k is wavenumber of surface waves, x'' is the distance from scatterer to receiver and Δx is the differential propagating distance between the direct incoming wave arriving at the receiver and the wave arriving at the scatterer (Fig. 1); R and R'' are receiver polarization vectors for direct incoming waves and scattered waves respectively. Since we use the vertical component of Rayleigh waves in this study, the receiver vectors R and R'' are equal.

The sensitivity kernels in eqs (3) and (4) are formulated for single-frequency observables of phase and amplitude from unwindowed seismograms in the time domain. The 2-D geometry of the single-frequency sensitivity kernels depends on wave frequency and reference phase velocity. In realistic data processing, Rayleigh waves are isolated from observed seismograms by applying proper time windows to the seismograms. The windowing of seismograms in the time domain is equivalent to smoothing the spectrum in the frequency domain. Thus the sensitivity kernels for windowed seismograms will be the integral of sensitivity kernels over a range of different frequencies centred at the frequency of interest. An example of sensitivity kernels for a waveform at the period of 50 s windowed using a 300 s window with a half cosine taper of 50 s on each end is shown in Fig. 2. In the inverse method we describe later, we interpolate velocities between nodal points with a 2-D Gaussian averaging function, thus implicitly restricting the scale of heterogeneities allowed through the characteristic length of the Gaussian filter. Here we also smooth the sensitivity kernels with a 2-D Gaussian average function to represent the distributed effects of any perturbation in the value of a node. In the example shown, we use a characteristic 1/e fall off distance of 50 km. The smoothing of the sensitivity kernels is necessary since we invert for phase-velocity coefficients at all nodal points instead of phase velocities directly. These phase-velocity coefficients are used to interpolate phase velocities at any position including at the nodal points; if the value of the coefficient is changed at one nodal point, it will affect the model velocities over a wide region through the Gaussian weighting function. In effect, these kernels are showing the sensitivity to phase velocity coefficients at nodal points rather than to the phase velocities at individual points.

The receiver is located at the origin (0, 0) and a plane Rayleigh wave propagates from left to right as indicated by the arrow. Obviously, the sensitivity is not limited to the ray path as is assumed in traditionally linearized ray tomography. The sensitivity kernels have a broad distribution and become broader with increasing distance from the station along the ray path. The sensitivity is mainly concentrated in the region of the first two Fresnel zones, and quickly decreases in the higher-order Fresnel zones, due to the interference between sensitivity kernels for different frequencies and the Gaussian smoothing. The magnitude of sensitivity is much larger in the area close to station than in the area away from station, which helps us to obtain high spatial resolution of phase velocity in regional tomography.

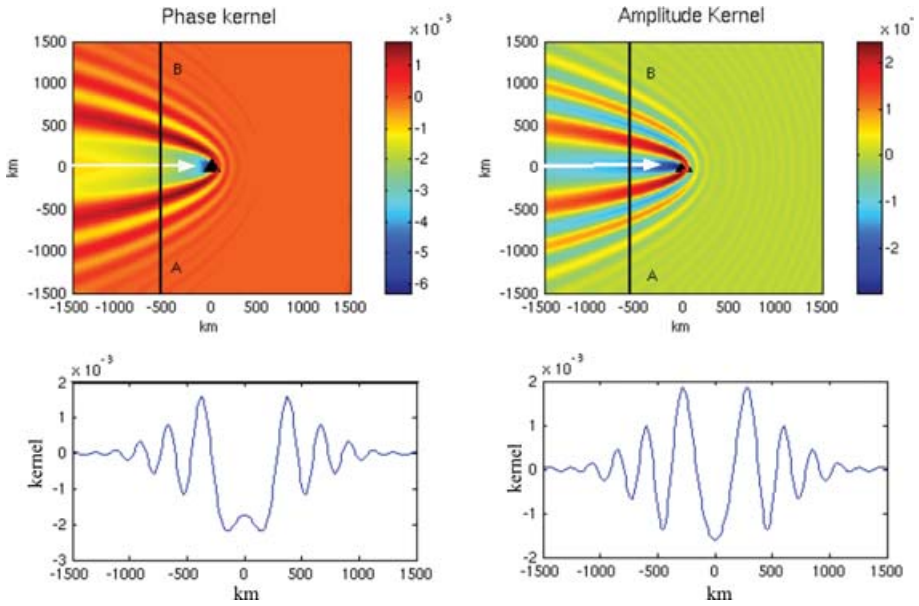

Figure 2. 2-D sensitivity kernels K_c^{ϕ}, K_c^{A} for a 20 mHz plane Rayleigh wave. (Top panels) map view of kernels at surface. Black triangles denote receivers; white arrows indicate the incoming direction of plane Rayleigh waves. (Bottom panels) Cross-section profile of kernels along line AB.

ACCURACY EVALUATION OF 2-D SENSITIVITY KERNELS

One of our primary goals in this paper is to evaluate how accurately the 2-D sensitivity kernels based on the Born approximation can represent wavefield variations caused by finite amplitude heterogeneities with dimensions on the order of a wavelength. In this section, we will evaluate this accuracy by comparing with numerical simulation.

Numerical simulation

The numerical simulation method we adopt to simulate surface wave propagation is a pseudo-spectral method developed by Hung & Forsyth (1998). This method solves a velocity-stress formulation of the elastic wave equation. Spatial variations of velocity and stress fields propagating in heterogeneous media are calculated by high-accuracy Fourier series in horizontal directions and by a Chebyshev differential operator in the vertical direction. A fourth-order Runge-Kutta method is used to represent time marching of wavefields. The computation programs are run in a high-performance parallel computer at the Technology Center for Advanced Scientific Computing and Visualization at Brown University.

In simulating Rayleigh wave propagation, we do the simplest case with a 2-D variable media in 3-D model space, that is, medium parameters are uniform in the vertical direction. We discretize a model space into a 288 × 288 × 64 grid with grid spacing of 20 km in the horizontal directions and an average of 10 km vertically. Thus the model space is 5740 km in the horizontal direction and 630 km in the vertical direction. Absorbing boundary conditions are applied at the sides and bottom of the model space. Isotropic medium properties are specified with *P*-wave velocity 8 km s^{-1}, S-wave velocity 4.5 km s^{-1} and density 3.3 kg m^{-3}. An inclusion cylinder is centred at the grid point of (2600 km, 2600 km) with radius of 100 km. In the interior of the inclusion cylinder, both *P*-wave and *S*-wave velocity are increased by 5 per cent, while density remains the same. Thus the corresponding phase velocity is increased by about 5 per cent as well. Rayleigh wave phase velocities calculated analytically (Saito 1988) for 1-D media are 4.15 km s^{-1} in the exterior and 4.36 km s^{-1} in the interior of the inclusion cylinder. As shown in Fig. 3, an initial plane Rayleigh wave propagates past the cylindrical anomaly from left to right, starting at 1000 km. The form of the starting wave is determined by first propagating waves for several thousand km from a point source in a homogenous model, then filtering and windowing to isolate the velocity and stress fields of the Rayleigh waves. 1891 'stations' are placed in each grid node to record particle motion in a neighboring subarea of 1200 × 600 km surrounding the inclusion cylinder. In the example shown in Fig. 4, the

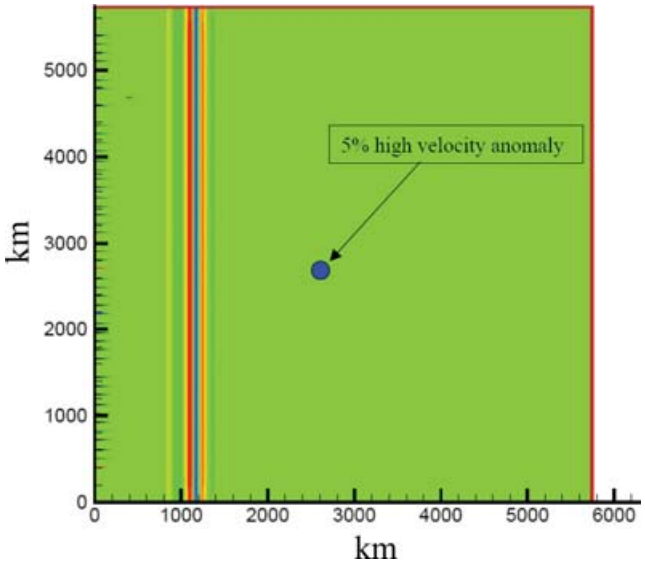

Figure 3. Model space for numerical simulation. Isotropic medium properties are specified with *P*-wave velocity 8 km s^{-1}, *S*-wave velocity 4.62 km s^{-1} and density 3.3 kg m^{-3}. The circle in the middle is a 5 per cent high velocity anomaly. The coloured strips in the left indicate the initial wave front of a plane Rayleigh wave on the surface.

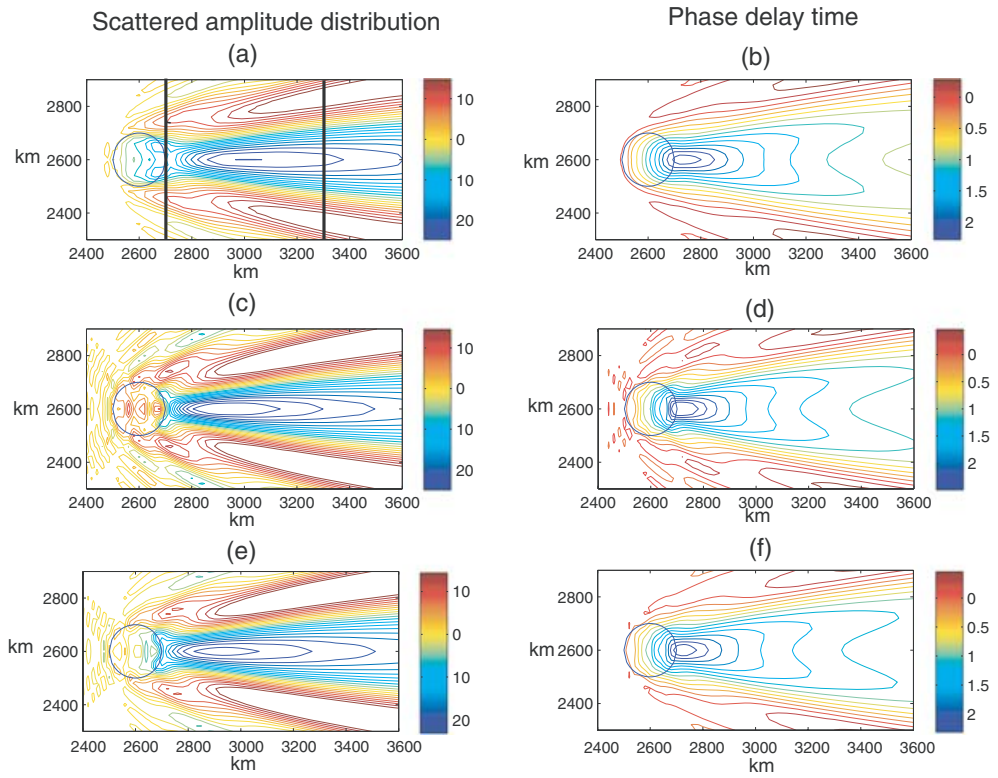

Figure 4. Scattered wavefields at 40 mHz by a 5 per cent high velocity cylinder marked with circle. Left panels: scattered amplitude distribution in percentage relative to a uniform wavefield. Right panels: distribution of phase delay time in seconds induced by the cylindrical anomaly. The direction of incidence is from left to right. (a) and (b): scattered wavefields from numerical simulation. (c) and (d): scattered wavefields from calculation based on 2-D sensitivity kernels with isotropic forward scattering approximation.(e) and (f): scattered wavefields from calculation based on 2-D sensitivity kernels with anisotropic scattering pattern as in Fig. 6. The two bold lines in (a) delineate the positions of two profiles along which cross-sections of amplitude and phase delay are plotted in Fig. 5.

seismograms recorded at each station are filtered using a band-pass filter with 10 mHz width centring at frequency of 40 mHz and windowed using the same time window as that used to calculate the sensitivity kernels, i.e. 300 s length with 50 s cosine taper. The filtered and windowed seismograms are transformed into the frequency domain to obtain phase and amplitude data. Thus in this example, we study scattering of surface waves with wavelength about 100 km propagating over a heterogeneous structure with scale about twice the wavelength. Since horizontal components are strongly influenced by higher mode Rayleigh waves and Love waves, we only consider the vertical components here.

In order to reduce the numerical errors introduced by the 3-D pseudo-spectral method, we do an additional simulation with the same model space but having uniform medium properties. In theory, for this uniform media, amplitude should be identical anywhere on the surface. However, due to numerical inaccuracy in representing the wave, there are some slight variations in amplitude that are a systematic function of position within the grid. These oscillations are nearly the same in models with introduced heterogeneities (at least with perturbations on the order of 5 per cent), so we find that we can reduce the numerical artifacts by simply subtracting the phase and amplitude data in the uniform case from those in cases with introduced heterogeneities. The retrieved phase and amplitude are the scattered phase and amplitude data caused by the included cylinder.

Wavefield comparison with calculation based on 2-D sensitivity kernels

With the same model space and station configuration as that in the numerical simulation, we also calculate the scattered phase and amplitude caused by the inclusion cylinder using 2-D sensitivity kernel, eqs (2), (3) and (4), for windowed Rayleigh waves at period of 40 mHz. This calculation based on 2-D sensitivity kernels only considers scattering of fundamental mode Rayleigh wave onto itself using a far-field approximation, whereas the numerical simulation includes all higher mode excitation and near-field terms. Friederich *et al.* (1993) have shown that the contribution of higher modes to the overall wavefield is negligible for a cylindrical structure situated in the centre of a homogenous structure. Thus we can approximately regard the simulation wavefield as a fundamental mode surface wave wavefield, and compare the wavefield based on 2-D sensitivity kernels directly with that from the numerical simulation.

In Fig. 4, we show the scattered wavefields in terms of phase and amplitude for period of 25 s based on the numerical simulation (Figs 4a and b) and the 2-D sensitivity kernels (Figs 4c–f). The circle represents the inclusion cylinder. Overall scattering patterns are very similar behind the cylindrical scatterer except that the extreme values in the focusing region at large distance are slightly overestimated by the scattering kernels and the width of the Fresnel zone is slightly underestimated (Fig. 5c), probably because there is a slight mismatch between the shape of spectrum for the simulation and that assumed in the sensitivity kernels.

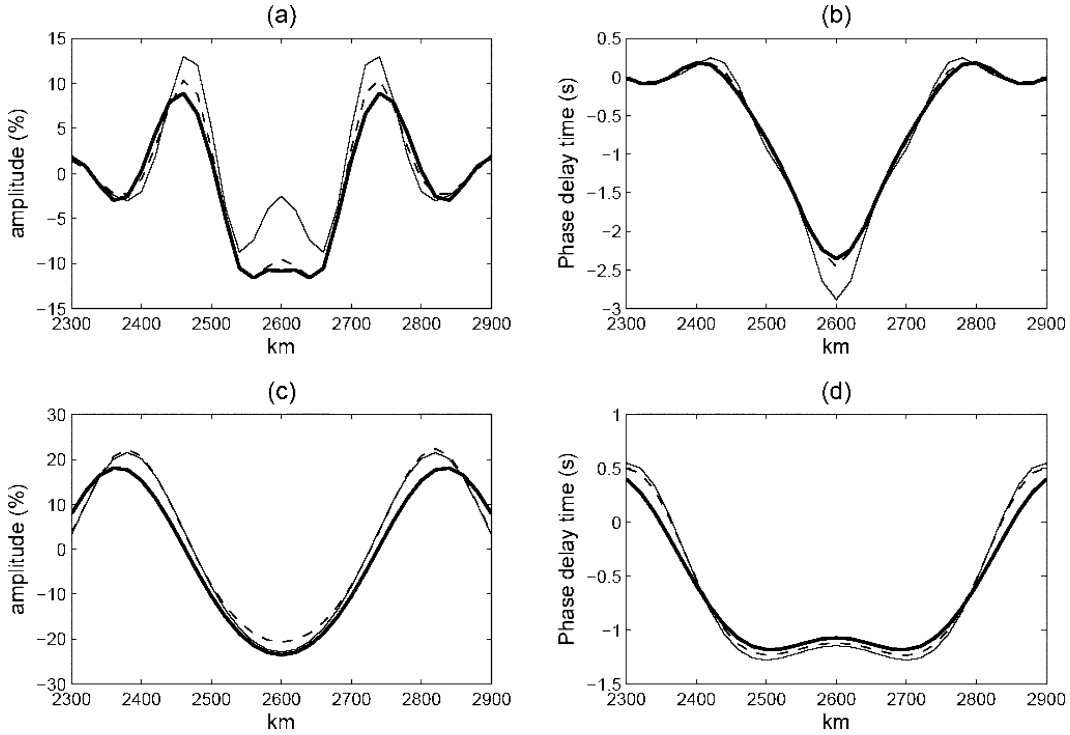

Figure 5. Cross-sections of amplitude and phase delay time along two profiles delineated in Fig. 4(a). (a) and (b) for the profile at $x = 2700$ km, the very end of the circle; (c) and (d) for the other profile at $x = 3300$ km, 600 km away from the circle. Bold lines represent numerical simulation case; thin solid lines represent the calculation based on sensitivity kernels with isotropic scattering pattern; and dashed lines represent the calculation with anisotropic scattering pattern (Fig. 6).

In the neighboring area of the circle, the difference of wavefields becomes larger. Figs 5(a) and (b) shows that amplitude and phase estimated from the scattering kernels are significantly different from the numerical simulation on a profile just past the heterogeneity. The difference is probably the result of the forward scattering approximation used in calculating the sensitivity kernels. The forward scattering approximation assumes scattering magnitude is the same in all directions. In reality, scattering is direction-dependent and determined by the perturbation of medium parameters, $\delta\alpha$, $\delta\beta$, $\delta\rho$. The scattering pattern at different depths can be calculated according to the formula (29d) in Snieder (1986). The Rayleigh wave at an individual period is sensitive to Earth structure over a range of depths. The largest sensitivity to shear velocity perturbations is located at a depth of about one third of the wavelength. Fig. 6 shows the radiation pattern of scattering at a variety of depths over the primary sensitivity range for Rayleigh waves with period of 25 s, assuming that the medium is a Poisson solid. We note that the patterns over this range of depths are similar in the forward direction, and there is some difference in the backward direction. If we intend to get the exact sensitivity to perturbations of local phase velocities, we need to do a numerical integral of scattering coefficients over depth, which requires prior knowledge of the form of the perturbations in elastic parameters in a forward model and will introduce cumbersome computations. Thus, as an approximation, we use the scattering pattern at the most sensitive depth as the overall scattering pattern when calculating sensitivity kernels considering scattering coefficients.

Figs 4(e) and (f) show the wavefield calculated using 2-D sensitivity kernels including the scattering pattern. This wavefield matches the scattered wavefield from numerical simulation better than those calculated using kernels without the scattering pattern, especially in the region close to the circle, which is obvious in the cross-sections in Fig. 5. For cross-sections right behind the circle, both amplitude and phase calculated with sensitivity kernels and anisotropic scattering pattern (dashed line) fit the numerical simulation (bold line) almost completely. For the cross-sections far away from the scatterer, there is only a small difference between the isotropic scattering (thin solid line) and angle-dependent scattering (dashed line), which is expected since the scattering angle from the forward direction is very small for stations far behind the cylindrical scatterer.

In 1993, Friederich *et al.* showed that multiple scattering is superior to the single-scattering method if the scattering region is bigger than one wavelength. In our case, the scatterer is almost twice as large as the wavelength for 25 s. Thus we expected that multiple scattering would have a significant contribution to the wavefield. However our calculation shows that the multiple scattering introduces only a very small amplitude effect, which is negligible compared to the overall scattering amplitude with a 5 per cent velocity perturbation. The possible reason for the large difference of amplitude between the single and multiple scattering in Friederich's study may be that they do not consider radiation pattern of scattering. As shown in Fig. 5, the isotropic single scattering (dotted line) predicts bigger amplitude right behind the circle than the numerical simulation (solid line), which is similar to the observed difference between single scattering and the numerical calculation in their paper. Thus we conclude that the single scattering method with non-isotropic scattering pattern is relatively accurate even for structure bigger than one wavelength, and multiple scattering is negligible for this simple example. Single scattering is linear with respect to phase velocity perturbation, which allows us to invert phase velocity with a linear inversion algorithm.

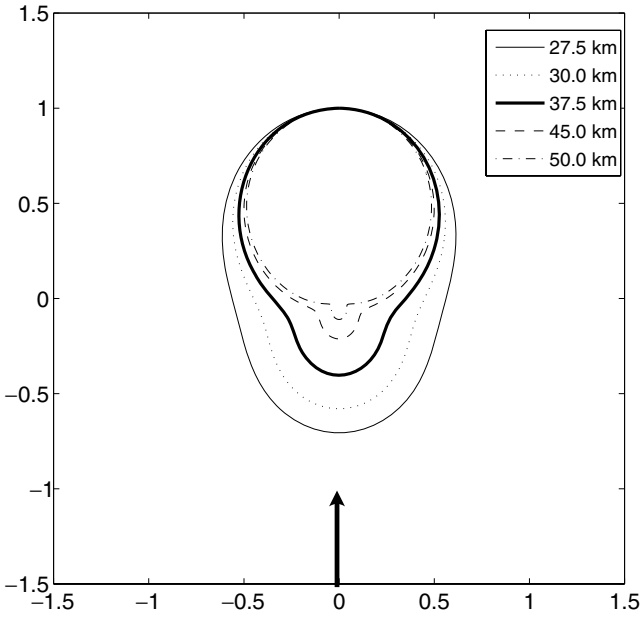

Figure 6. Radiation pattern for a scatterer located at the origin. The scattering is fundamental mode to fundamental mode of Rayleigh wave at period of 25 s for *P*- and *S*-wave heterogeneities, assuming the medium is a Poisson solid. The wave is incident in direction indicated by arrow. Radiation patterns at different depths are represented with different style lines, which are shown in legend. Note that bold line presents the pattern at the most sensitive depth.

We also note that the amplitudes calculated from scattering kernels inside the circle are generally larger than those from the numerical simulation. Three cross-section profiles of amplitude and phase at the longitudinal profile through the centre of the circle and 20 km from the centre in either direction are shown in Fig. 7. The predicted phase matches the numerical simulation very well except for a small discrepancy in the middle of the circle. The amplitude is systematically higher than the numerical simulation solution inside the circle, but agrees closely with the numerical simulation solution outside the circle along all three profiles. The reason for the amplitude mismatch when anisotropic kernels are employed is primarily the station site responses in the numerical simulation that are neglected in the 2-D sensitivity kernels. When isotropic scattering is assumed, the discrepancy inside the anomaly is even greater due to an overestimation of the intensity of backscattering (compare Figs 4a and c). Since the phase velocity is about 5 per cent higher inside the circle than outside, the wavelength is about 5 per cent greater, and the vertical energy distribution of Rayleigh waves will be different inside and outside the circle. The anomalous cylindrical structure with higher phase velocity tends to have less energy concentrated at shallow depth than the background media, which leads to smaller amplitude observed at the surface than that predicted using 2-D sensitivity kernels that have no station site response term.

In order to demonstrate that this amplitude difference is caused by local structure, we do a numerical experiment in which a plane Rayleigh wave propagates through two uniform structures with 5 per cent percent phase velocity contrast from left to right. A number of stations are placed along a line perpendicular to the medium boundary. We note that the amplitude is about 5 per cent lower in the higher phase velocity region than in the lower phase velocity space and the transition of amplitude across the boundary is gradual (Fig. 8). This amplitude variation across the boundary is due to local structure beneath stations, which we call the station site response. In order to take the station site response into account in surface wave tomography, we need an additional amplitude parameter for each station analogous to station static corrections for time delays, except that this site response term will be frequency dependent. In principle, if we used complete 3-D response kernels instead of 2-D kernels, the site response term might be unnecessary to represent the local amplitude response. In practice, however, 3-D kernels would greatly increase the difficulty of the inverse problem for structure, because they would require the simultaneous inversion of all periods for 3-D velocity structure. Our current inverse approach, described below and in Forsyth & Li (2005) and Yang & Forsyth (2005, submitted) inverts for 2-D phase velocity variations one period at a time and allows for a simple representation of the structure of the incoming wavefield. In addition, station site response terms would be required anyway, because it is necessary to allow for incorrect instrument responses and for the effects of shallow structure that would be unresolvable with the period range employed in typical regional studies using teleseismic sources.

SURFACE WAVE INVERSION

Resolution evaluation

In previous regional surface wave inversions, we approximated scattering effects from heterogeneities outside the vicinity of the array by representing the incoming wave with two interfering plane waves (Forsyth & Li 2005). The interference of two plane waves produces a sinusoidal variation in amplitude that is a reasonable first-order approximation over an array of limited extent downrange from a scatterer. In the vicinity of the array, phase effects of heterogeneities were considered, but amplitude effects were neglected. Finite frequency effects were approximated with a Gaussian phase sensitivity function, which assumes the sensitivities of Rayleigh waves to heterogeneous structure are equal along the ray path but decays as a 1-D Gaussian function in the direction perpendicular to the ray path. The characteristic length for the 1-D Gaussian function is determined from the width of the first Fresnel zone at a distance characteristic of the dimension of the array. The choice of the characteristic length was discussed in detail by Weeraratne *et al.* (2003). The primary disadvantage of this representation of the sensitivity is that it neglects the great increase in phase sensitivity as the Fresnel zone narrows near the receiver. In this study, we continue to represent the effect of distant scatterers with two incoming plane waves, but represent the effects of finite frequencies for each incoming wave with 2-D sensitivity kernels calculated with the Born approximation. Sensitivity of both phase and amplitude to heterogeneous structure is considered, whereas only phase sensitivity was considered in the previous method. Thus the new method with 2-D sensitivity kernels should improve the spatial resolution of phase velocity greatly.

In order to demonstrate the inversion resolution of the new method based on 2-D sensitivity kernels and compare with the previous method based on Gaussian sensitivity function, we apply both methods to seismic data synthesized using the pseudo-spectral method to invert for phase velocity.

We put a 1000 × 600 km subregion in the middle of a model space with dimensions 5740 × 5740 km. The subregion is a smoothed checkerboard structure with 200 km square anomalies. Both *P*-wave velocity and *S*-wave velocity alternate fast and slow anomalies of ±5 per cent. A 60-station network with station spacing 120 km is placed inside the checkerboard structure (Fig. 9a). A number of

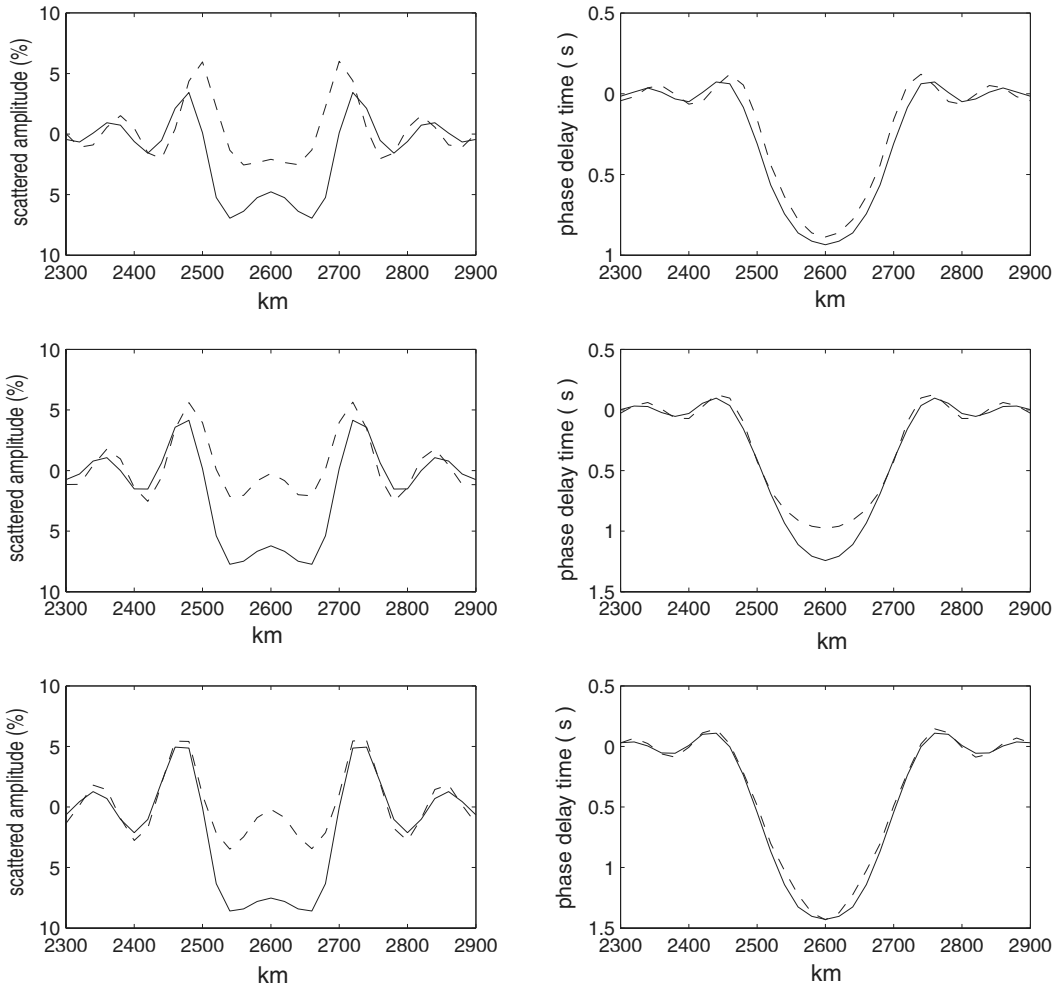

Figure 7. Cross-section of amplitude (left panels) and phase delay time (right panels) along three profiles. Middle panels for the profile at the centre of the circle, top panels for the profile 20 km left of the centre, and bottom panels for the profile 20 km right of the centre. Solid lines represent numerical simulation case (Figs 4a and b); dashed lines represent the calculation based on sensitivity kernels with anisotropic scattering pattern (Figs 4d and f).

plane waves propagate over the checkerboard structure from different directions with even azimuthal distribution at an interval of 15 degrees. Even though each incoming wave front in this numerical experiment is a single plane wave because there are no external heterogeneities, we can still use the two-plane wave method; the inversion will simply find a solution in which each incoming wave is represented with one main plane wave with large amplitude and a second plane wave with very small amplitude. In the inversion, 6 wavefield parameters are required for each incoming wave, describing the amplitude, initial phase and direction of propagation of each of the two plane waves. To isolate the fundamental mode Rayleigh waves, the same data processing procedure of filtering and windowing as that used in preceding section are applied to the synthesized seismograms. In the inversion, we parametrize the study region with 273 velocity nodes distributed evenly inside the checkerboard region with spacing 50 km and an additional 152 nodes surrounding the checkerboard to represent some of the effects from outside the array for later experiments. The phase velocity at any point in the study region is represented by a 2-D weighted average of the values at nearby grid nodes using a Gaussian weighting function with 80 km characteristic length. The same function is employed in smoothing the Born sensitivity kernels. We add a multiplicative amplitude correction factor or site response term to be determined for each station. To invert phase and amplitude data for phase velocity at each node, the incoming wavefield parameters and the site terms simultaneously, a standard, iterative, linearized inversion technique (Tarantola & Valette 1982) is utilized, alternating with a simulated annealing adjustment of the wavefield parameters (Forsyth & Li 2004). The solution for the general non-linear least-squares problem is

$$\Delta m = \left(G^T C_{nn}^{-1} G + C_{mm}^{-1}\right)^{-1} \left(G^T C_{nn}^{-1} \Delta d - C_{mm}^{-1} [m - m_0]\right) \qquad (5)$$

where m_0 is the original staring model, m is the current model, Δm is the change relative to the current model, Δd is the difference between the observed and predicted data for the current model, $\mathbf{G}$ is the partial derivative of $\mathbf{d}$ with respect to perturbation of m, $\mathbf{C}_{\rm nn}$ is data covariance matrix describing the data uncertainties, and $\mathbf{C}_{\rm mm}$ is the prior model covariance matrix, which acts to damp or regularize the solution. The uncertainties of synthesized data, which are introduced due to the inaccuracy of the numerical simulation, are relatively small compared to a real data set. However, we can approximately regard the synthesized data as a realistic data set by

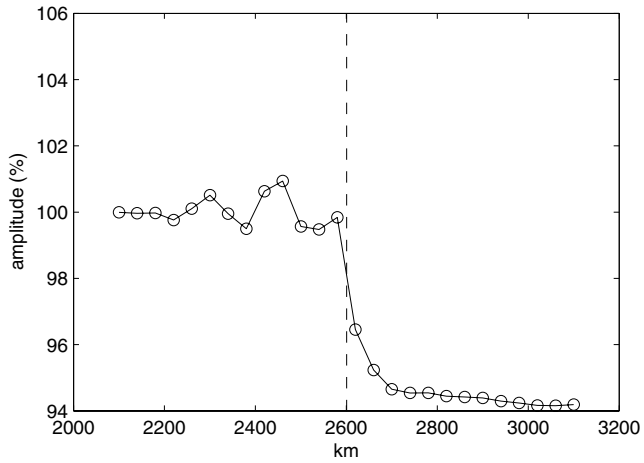

Figure 8. Amplitude at each station placed along a line perpendicular to the medium boundary. The dashed line indicates the boundary position. Note that amplitude in higher velocity region is smaller, but the transition is not instantaneous. The case shown is for 25 s period with wavelength about 100 km.

assigning values of data uncertainties in the diagonal terms of C_{nn} that are typical of those found in regional surface wave studies (Li *et al.* 2003, 2005; Weeraratne *et al.* 2003). To damp the underdetermined solution and stabilize the inversion, we employ a prior model covariance of 0.4 km s^{-1} for phase velocity parameters. The choice of damping value 0.4 km s^{-1} for phase velocity parameters is based on many experiments using a range of damping values from 0.2 to 0.5 km s^{-1} by considering the trade-off between the resolution and model uncertainties.

The resultant phase velocity maps based on the 2-D sensitivity kernels are shown in Fig. 9 at periods of 25 s (Fig. 9a), 50 s (Fig. 9c) and 100 s (Fig. 9d). One phase velocity map at the period of 25 s based on Gaussian sensitivity function is shown in Fig. 9(b). The characteristic length of Gaussian sensitivity function for this figure is 80 km, which yields a sensitivity function that approximately represents the average width of the first Fresnel zones of the 2-D finite frequency sensitivity kernels for waves propagating across the study region. For the inversion based on 2-D sensitivity kernels, anomalies of phase velocity are almost completely recovered at the periods of 25 and 50 s. At the period of 100 s, we still can recover the variation pattern, although the magnitude of anomalies is greatly underestimated. The underestimation in magnitude is partly due to the wide Fresnel zone of long-period surface waves, which decreases

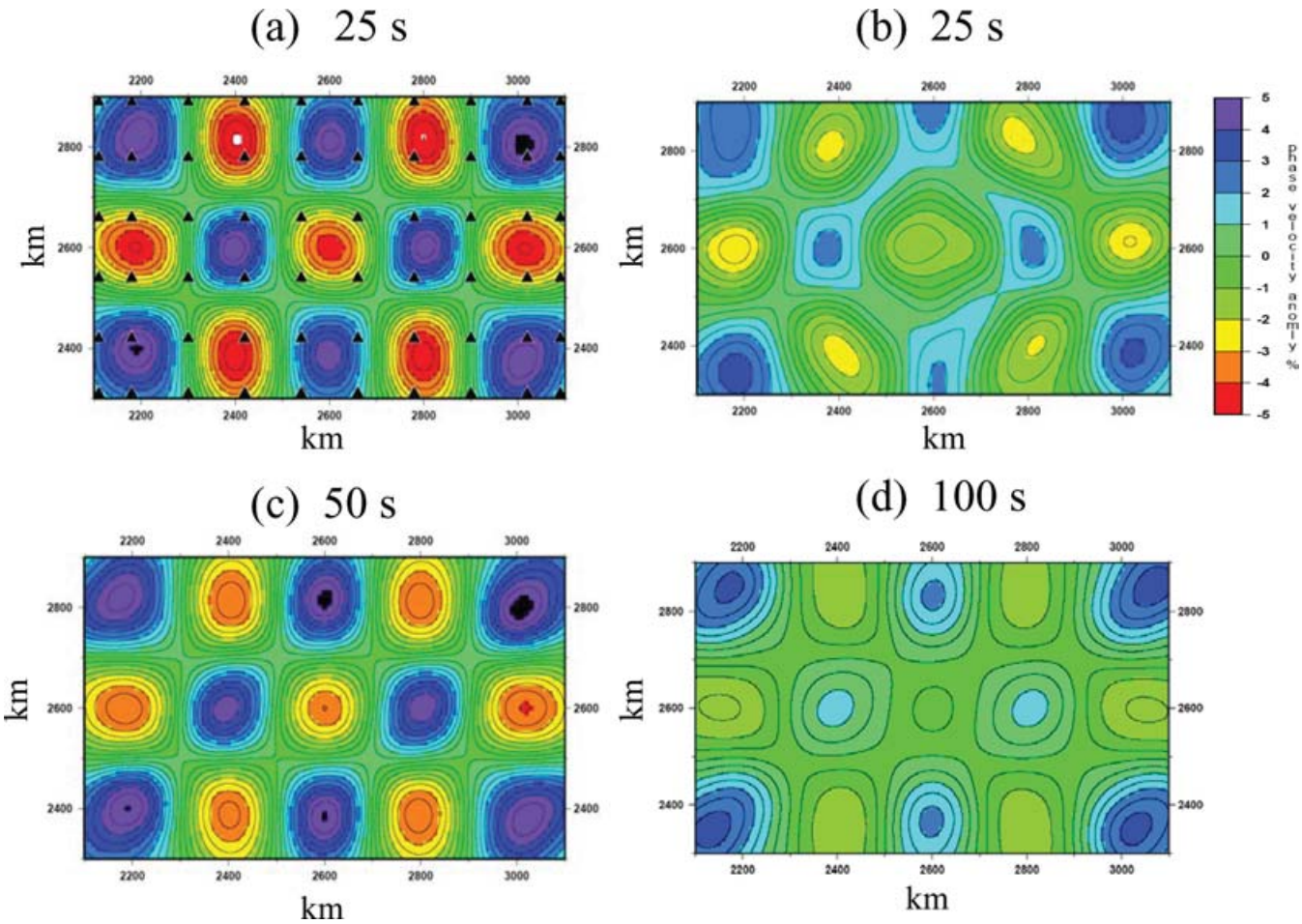

Figure 9. Recovered phase velocity maps for checkerboard structure based on the 2-D sensitivity kernels at periods of 25 s (a), 50 s (c) and 100 s (d). For comparison, (b) shows the recovered phase velocity map at period of 25 s based on Guassian sensitivity function. Black triangles in Fig. 9(a) represent stations put at the surface in numerical simulation for phase velocity inversion.

the local intensity of the sensitivity functions, and the damping that reduces the amplitude of the anomalies when the sensitivity is low. The primary limitation is not the accuracy of the kernels when the wavelength is similar to the wavelength of the heterogeneities; it is the increased uncertainty in relative arrival time at longer periods coupled with the decreased local sensitivity. In the absence of noise, damping would be unnecessary and the pattern could be recovered nearly perfectly at all periods. For the inversion based on Gaussian sensitivity function, the pattern of anomalies can only be recovered fairly at the period of 25 s. At longer period, the anomalies are poorly imaged and the primary limitation is the accuracy of the Gaussian representations of the kernels close to the stations.

These inversion experiments demonstrate that inversion based on 2-D single-scattering sensitivity kernels can greatly improve phase velocity resolution compared to that based on Gaussian sensitivity function. The new inversion method can resolve structure on the scale of one wavelength given the distribution of stations and events in the experiment. The improvement in resolution helps us to recover the Earth's smaller-scale structure. In a tomographic study, equivalent fits to the phase data might be achievable using ray theory with time or phase delays confined to the narrow ray paths, provided damping was reduced or smaller-scale structures were allowed. However, the approach we use allows the consistent use of amplitude and phase data with some natural damping built in by the finite width of the response kernels.

The improvement in resolution in this study is much larger than found by Sieminski *et al.* (2004). Sieminski *et al.* (2004) showed that surface wave tomography based on ray theory with dense path coverage of the target region and Gaussian sensitivity kernels can resolve structure almost as well as tomography based on finite-frequency sensitivity kernels. The primary reasons for the difference in our conclusions are the differences in the location of target anomalies and the scale of the study region. Our study region is much smaller than that in Sieminski *et al.* (2004) and our anomaly structure is close to the stations, while the test anomalies in Sieminski *et al.* (2004) are far from both the events and stations and the paths are several tens of degrees in length. Since the finite-frequency kernels change rapidly near both ends of a ray path, a Gaussian sensitivity function with uniform width along the ray path cannot describe adequately the increase in sensitivity or the shape of the sensitive region as the Fresnel zone narrows close to the station. Far from the station, a Gaussian sensitivity function based on the average or maximum width of the Fresnel zone may be a reasonable approximation, but as we have demonstrated here, it is not sufficient for tomography within a regional array when the anomaly scale is on the order of a wavelength. The second reason for the larger improvement in our study is that we incorporate amplitude kernels with amplitude data in our tomography, while only phase data were used in Sieminski *et al.* (2004). The improvement in resolution attributed to amplitude data is shown in the following section.

Importance of amplitude in surface wave tomography

In the above section, we have shown that the new inversion method including both phase and amplitude sensitivities can greatly improve the resolution of phase velocities. In this section, we will evaluate the importance of amplitude information in the inversion for phase velocities and show why we should include amplitude data in surface wave tomography.

Conventional surface wave tomography uses only phase data to invert for phase velocities. Amplitude has been long neglected in tomography since amplitude is affected by many different factors, such as scattering, attenuation, station response and local structure. It is hard to estimate all the different effects in tomography with ray theory. However amplitude contains important information about Earth structure and should be combined with phase data to better constrain Earth structure. As demonstrated in a previous section, amplitude variations caused by scattering can be estimated accurately by the amplitude sensitivity kernel when Rayleigh waves propagate over inhomogeneous structure. Anelastic effects on amplitude are not considered here, since we can model surface wave propagation only in elastic media using the pseudo-spectral method. However the anelastic effect, i.e. attenuation, can be estimated easily in tomography based on the propagation distance of individual wave rays and the effects are relatively small in an array of limited extent. Applying the new tomography method to Rayleigh wave data recorded at the Trinet network in southern California, Yang & Forsyth (2005) showed that amplitude variations caused by attenuation are much less than those caused by scattering in southern California and inversions with or without attenuation included result in almost identical phase velocity maps.

We invert phase and amplitude data separately for phase velocity perturbation using the appropriate sensitivity kernels. Model parameters and the inversion scheme are the same as in the combined inversion described in the previous paragraphs. Inversion results are shown in Fig. 10 at period of 50 s in comparison to the combined inversion. Inversion using only amplitude data or phase data can recover the variation pattern of anomalies, but the strength of anomalies are not recovered fully in both inversions. If we combine both amplitude and phase data in inversion, the anomalies can be almost perfectly recovered with realistic noise levels.

Although amplitudes clearly do not provide information about the absolute velocity, they appear to contain equivalent information as phase about perturbations in Earth structure. Phase or amplitude alone does not provide complete resolution, given realistic estimation of noise levels. In the real Earth situation, when a Rayleigh wave propagates along the ray path from source to receiver, it will be affected by heterogeneous structure off the ray path. The ray path may deviate from the great circle due to multipathing and scattering, leading to change of the direction of propagation and the presence of a non-planar incoming wavefield. In order to obtain the structural phase velocity, the non-planar incoming wavefield stemming from heterogeneities outside seismic array must be accounted for using both phase and amplitude information.

One-plane wave versus two-plane wave

Wielandt (1993) has shown that the inaccurate representation of incoming wavefields could bias the resolved phase velocity systematically from the real phase velocities. Friederich & Wielandt (1995) developed a method that can simultaneously solve for phase velocity variations within an array region and the incoming wavefield for each event. The incoming wavefields are represented by a series of basis functions in the form of Hermite-Gaussian functions. However due to many parameters used to represent the incoming wavefields, with this method it is hard to resolve relatively small changes in the wavefield associated with variation in phase velocity within the study area. In order to simplify the representation while taking into account the primary effects of non-planar energy, Forsyth & Li (2004) developed a two-plane-wave method, which uses two plane waves coming with different incoming directions to represent the variation of wavefield. This method has been

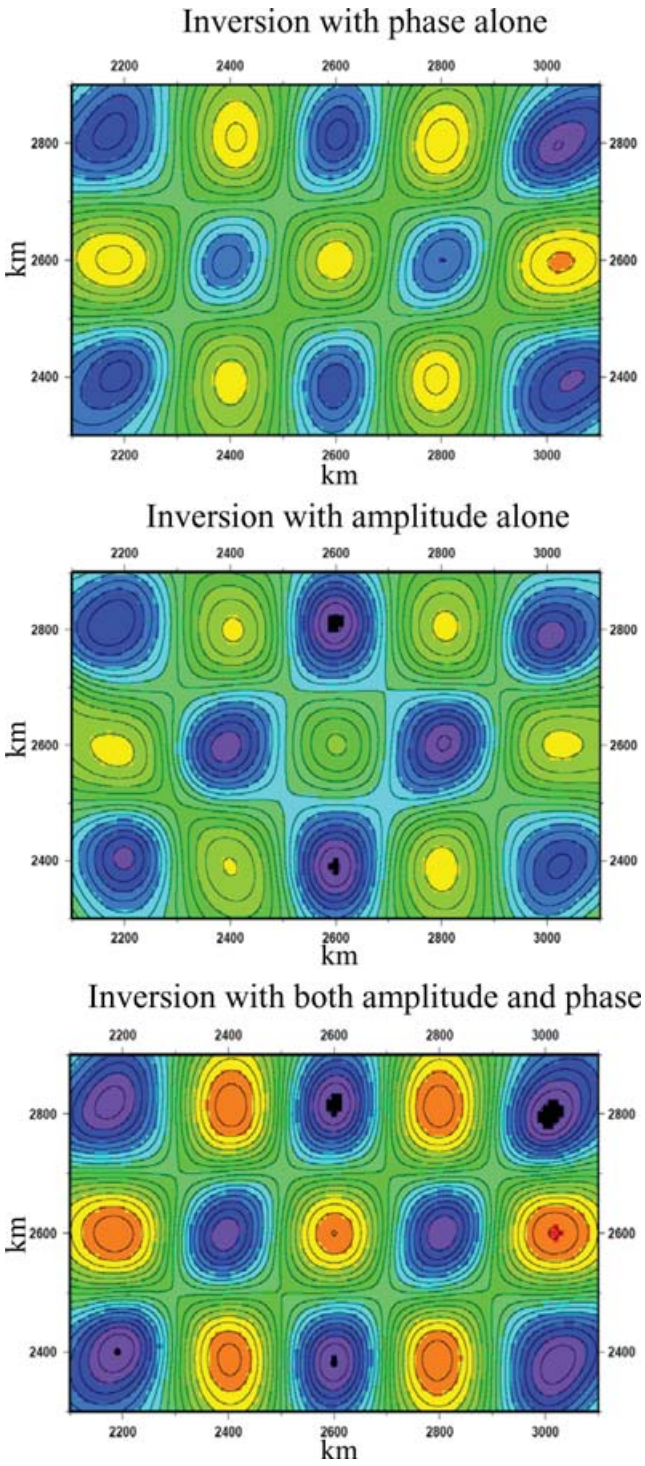

Figure 10. Recovered phase velocity maps at period of 50 s. (Top) inversion with phase data alone; (Middle) inversion with amplitude data alone; (Bottom) inversion with both amplitude and phase data.

used to represent incoming surface waves in several regional surface wave tomography studies (Forsyth *et al.* 1998; Li *et al.* 2003a,b; Weeraratne *et al.* 2004). Here we intend to illustrate the advantage of the two-plane-wave method in representing the wavefield and resolving phase velocity by numerical experiments.

We create a spatial model that has the same dimensions as that in preceding checkerboard experiment. A checkerboard structure is placed in the middle of the model space, and outside the checkerboard a random medium is constructed with characteristic scale about 100 to 200 km (Fig. 11). The strongest velocity anomalies in the random media are ± 5 per cent and the velocities of *P* and *S* waves change simultaneously with same percentage. In order to illustrate the influence of outside heterogeneous structure on the wavefield, we compute two kinds of wavefields just as Friederich *et al.* (1994) did in their study: one without local checkerboard structure, i.e. local structure is uniform, the other with local checkerboard structure. We show one example with a plane wave incident from the bottom of the diagram beginning at a distance of about 1500 km from the edge of the checkerboard. Amplitude is retrieved from stations put at each grid point and is shown in Fig. 12 at a period of 25 s. First, we can see that broad features of the amplitude distribution are similar for both cases with local checkerboard or without checkerboard, which implies that amplitude variation is mainly controlled by outside heterogeneities and local structure has a smaller influence on wavefield than the random media outside. Second, the range of amplitude variation is large, from 0.6 to 1.4. If we regard the incoming wave as a single plane wave, no amplitude variation is predicted inside the local structure in the case without checkerboard, which differs greatly from the real variation (Fig. 12b). In the entire 600 × 1000 km inner region, the non-plane waves can be better approximated with two plane-wave interference, as shown in the following paragraph.

To do inversion for local structure with surrounding random media, we first simulate wavefields propagating from different azimuths. The structure remains the same for all of these wavefields. 24 different wavefields are simulated with uniform azimuthal distribution at 15 degree intervals. The two-plane-wave method with sensitivity kernels from the Born approximation is applied to the phase and amplitude data. Recovered structure is shown in Fig. 13 for this case. The variation pattern of phase velocity is well recovered for both periods of 25 and 50 s. The shape of anomalies in some edge blocks is distorted, such as in the lower-right corner, due to the effects of heterogeneous structure just outside the boundary of the checkerboard region. In order to verify the advantage of two plane waves over one plane wave, we also do the same inversion for phase velocities at the period of 25 s regarding each incoming wave as one single plane wave. In both inversions, we include site response terms for each station, and in the single-plane-wave method, the direction of propagation for each event is a variable. By comparing the result of both inversions, we find that two-plane-wave method improves the fit to amplitude and phase data and reduces the rms misfit of both amplitude and phase by about 30 per cent. The two-plane-wave method based on sensitivity kernels can accurately resolve phase velocities within a seismic array even if there are large heterogeneities present outside the array area that produce amplitude variations larger than the variations associated with local structure, provided there is good azimuthal coverage.

A BRIEF PRACTICAL EXAMPLE

The primary goal of this study was to test whether, within the context of regional surface wave tomography, the 2-D Born approximation yields sensitivity kernels that adequately represent the response to a perturbation, including near receiver terms and multiple scattering effects that are part of the full elastic response. In that context, the answer is yes, provided that a static site response term is included when modelling amplitude variations. To demonstrate the accuracy,

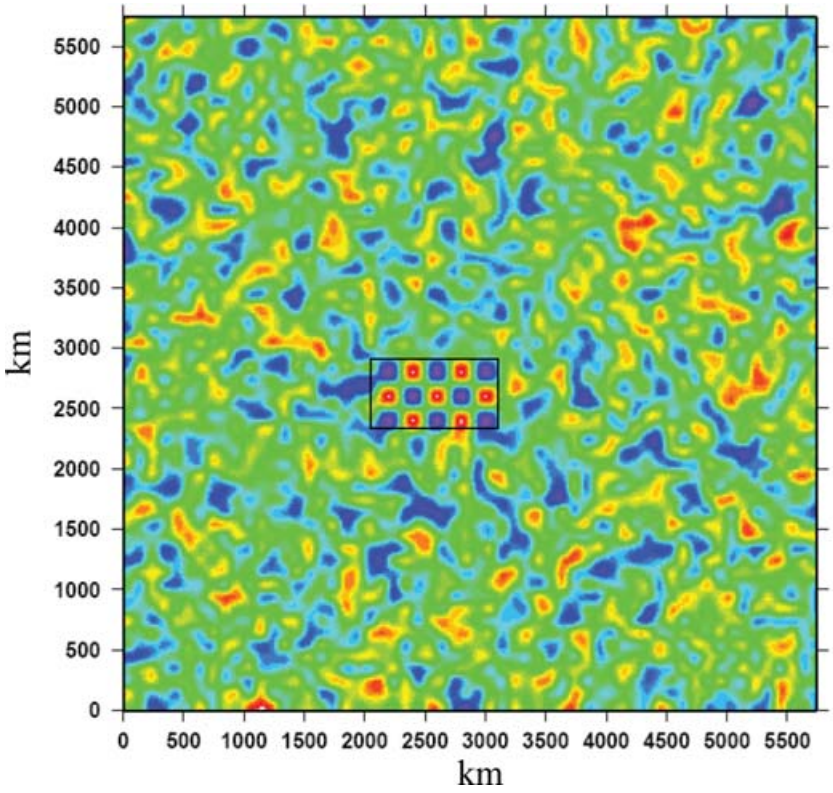

Figure 11. Constructed model space with random phase velocity. A checkerboard structure is emplaced in the middle delineated by a rectangle. The strongest velocity anomaly of random medium is 5 per cent and the typical scale of anomalies is about 100–200 km.

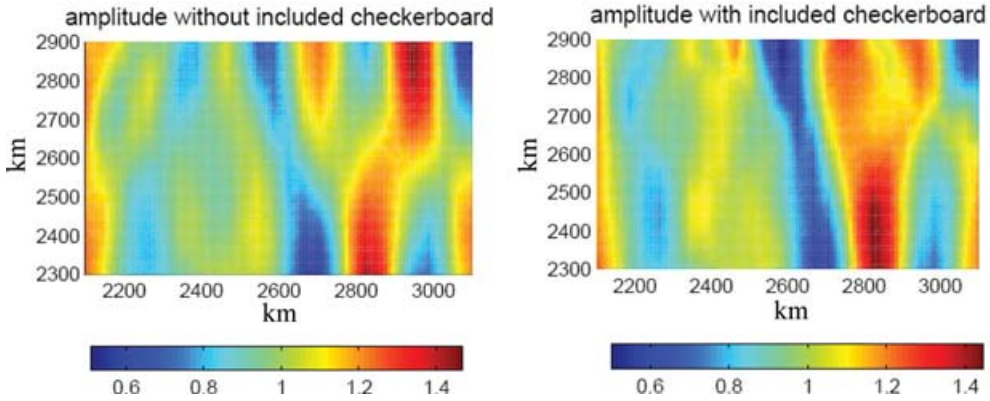

Figure 12. Amplitude distribution from numerical simulation for structure shown in Fig. 11. The displayed area is the rectangular region in Fig. 11. The direction of wave incidence is from bottom of diagram to top. Left panel shows amplitude distribution without included checkerboard structure; right panel shows amplitude distribution with included checkerboard structure.

we constructed synthetic models with known structure for direct examination of the response kernels and for use in hypothetical inverse problems with an array of detecting stations.

Although we cannot test the method using real data, because the structure is then unknown, we recognize that seismologists will not be convinced of its utility without a practical illustration of its application. In Yang & Forsyth (2005), we have applied the method in a tomographic study of southern California. That paper describes in detail the station or site corrections, inclusion of attenuation and azimuthal anisotropy, and all the practical difficulties one encounters in a real application. Here, in Fig. 14, we briefly illustrate the results for phase velocity variations at one period, 100 s. The azimuthal distribution of sources is very good, with the largest gap about 32 degrees. Other than this gap, the coverage is better than in our synthetic examples, with nearly 100 sources and stations that are typically 70 to 100 km apart in comparison to the 24 sources at 15 degree azimuth intervals with stations 120 km apart in the synthetic experiments. Consequently, the resolution is substantially better than the example in Fig. 9(d). We resolve velocity variations with scales down to about 125 km (wavelength about 250 km) using 100 s period Rayleigh waves that have a wavelength of about 400 km. Maximum velocity variations with the map area are about 6 per cent. Error analysis indicates that any variation greater than about 1.5 per cent is statistically significant at the 95 per cent

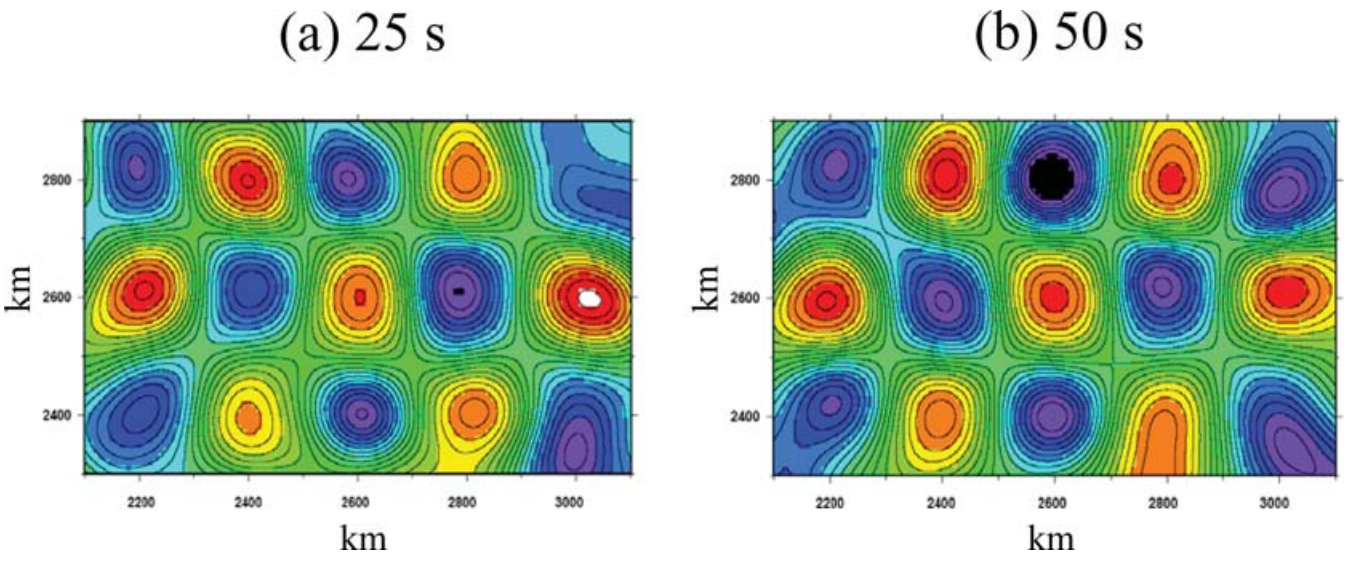

Figure 13. Recovered phase velocity maps for checkerboard structure with surrounding random media shown in Fig. 11 at periods of 25 s (a) and 50 s (b).

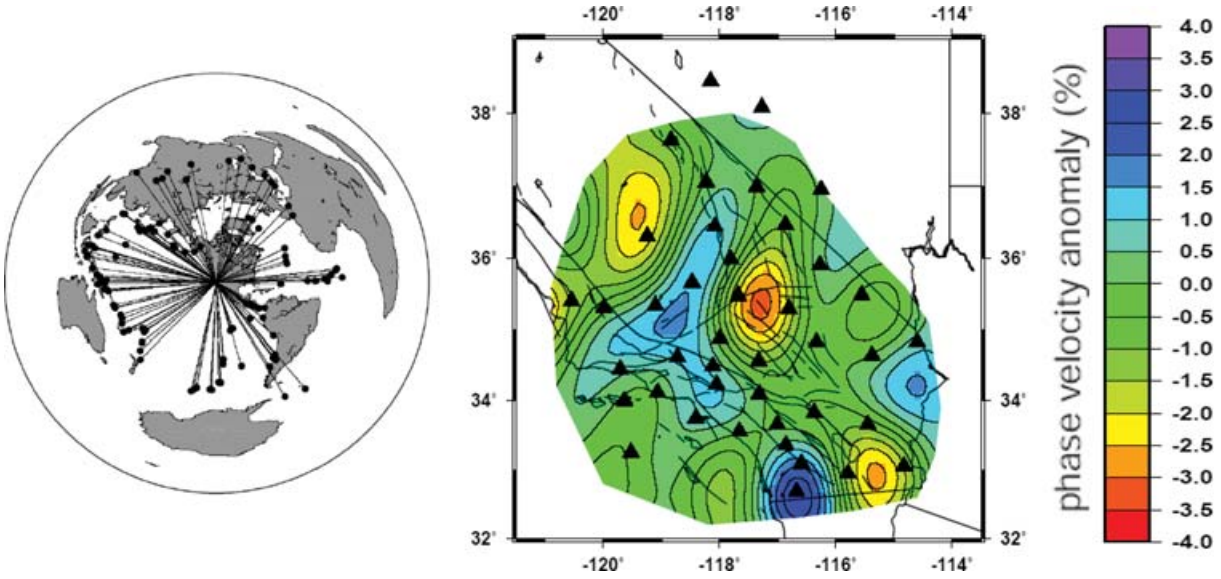

Figure 14. Phase velocity anomalies in southern California for Rayleigh waves at 100 s period (right). Distribution of sources is shown on azimuthal equidistant map (left). Station locations are shown by small triangles. Data is from Yang & Forsyth (2005).

confidence level. For further details and tectonic interpretation, see Yang & Forsyth (2005).

CONCLUSIONS

We have revised the 2-D Born approximation sensitivity kernels for the global case to that for a regional case with a plane-incoming wave. The 2-D sensitivity kernels for regional cases are used to calculate the scattered wavefield for Rayleigh wave propagation over a cylindrical anomaly. In order to assess the accuracy of 2-D sensitivity kernels in describing the wavefield variation induced by anomalous structure, we use the pseudo-spectral method to numerically simulate the Rayleigh wave propagation and compare it to the calculated wavefield based on sensitivity kernels. We found that 2-D sensitivity kernels with isotropic forward scattering approximation are not accurate enough to estimate the wavefield variations in regions close to anomalies. We can use the radiation pattern of scattering for the heterogeneities of *P*-wave and *S*-wave velocities at the depth of greatest sensitivity for Rayleigh waves as the overall scattering pattern to better model wavefield variations. Inside anomalies, the amplitude is significantly affected by local structure, which is not accounted for by the sensitivity kernel. Additional parameters should be introduced for each station in surface wave tomography to account these local structure effects. This local site effect on amplitude contains some information about structure beneath stations and will be studied further in the future.

Based on the 2-D sensitivity kernels, we develop a surface wave tomography method by representing the incoming waves as two plane waves. For each plane wave, the 2-D sensitivity kernels are employed to account for finite frequency effects. We synthesize Rayleigh wave propagation over checkerboard structure and apply the developed method to synthesized data to recover the input checkerboard structure. We found the method can almost completely recover the input structure when the size of anomalies is larger than

one wavelength. When the size of anomalies is about half the wavelength, we still can recover the pattern of variations of phase velocity, but the magnitude of anomalies is underestimated. The amplitude of surface waves is important data and contains nearly as much information about the Earth structure as phase data. We should combine both amplitude and phase data to constrain incoming wave fields and invert for phase velocity.

ACKNOWLEDGMENTS

We would like to thank Karen Fischer, Shu-Huei Hung and Ying Zhou for helpful discussions. We thank Guust Nolet and another anonymous reviewer for the critical and constructive comments. This research was supported by National Science Foundation grants OCE-9911729 and EAR-0510621.

REFERENCES

Clevede, E., Megnin, C., Romanowicz, B. & Lognonne, P., 2000. Seismic waveform modeling and surface wave tomography in a three-dimensional Earth: asymptotic and non-asymptotic approaches, *Phys. Earth planet. Int.,* **119,** 37–56.

Forsyth, D.W. & Li, A., 2005. Array-analysis of two-dimensional variations in surface wave phase velocity and azimuthal anisotropy in the presence of multi-pathing interferece, in *Seismic Earth: Array Analysis of Broadband Seismograms*, eds Levander, A. & Nolet, G., pp. 81–98, *Geophys. Monogr.,* **157,** AGU. Washington DC.

Forsyth, D.W., Webb, S., Dorman, L. & Shen, Y., 1998. Phase velocities of Rayleigh waves in the MELT experiment on the East Pacific Rise, *Science* **280,** 1235–1238.

Friederich, W. & Wielandt, E., 1995. Interpretation of seismic surface waves in regional networks: joint estimation of wavefield geometry and local phase velocity. Method and numerical tests, *Geophys. J. Int.,* **120,** 731–744.

Friederich, W., Wielandt, E. & Stange, S., 1993. Multiple forward scattering of surface waves: comparison with an exact solution and Born single-scattering methods, *Geophys. J. Int.,* **112,** 264–275.

Friederich, W., Wielandt, E. & Stange, S., 1994. Non-plane geometries of seismic surface wavefields and their implication for regional surface-wave tomography, *Geophys. J. Int.,* **119,** 931–948.

Hung, S.-H. & Forsyth, D.W., 1998. Modeling anisotropic wave propagation in oceanic inhomogeneous structures using the parallel multi-domain pseudo spectral method, *Geophys. J. Int.,* **133,** 726–740.

Li, A., Forsyth, D.W. & Fischer, K.M., 2003. Shear velocity structure and azimuthal anisotropy beneath eastern North America from Rayleigh wave inversion, *J. geophys. Res.,* **108**(B8), 2362, doi:10.1029/2002JB002259.

Li, A., Forsyth, D.W. & Fischer, K.M., 2005. Rayleigh wave constraints on shear-wave structure and azimuthal anisotropy beneath the Colorado Rocky Mountains, in *The Rocky Mountain Region: An Evolving Lithosphere,* eds Karlstrom, K.E. and Keller, G.R., pp. 385–401, *Geophys. Monogr.,* **154,** AGU. Washington DC.

Ritzwoller, M.H., Shapiro, N.M., Barmin, M.P. & Levshin, A.L., 2002. Global surface wave diffraction tomography, *J. geophys. Res.,* **107**(B12), 10.1029/2002JB001777.

Saito, M., 1988. DISPER80: A subroutine package for the calculation of seismic normal-mode solutions, in *Seismological Algorithms*, pp. 293–319, ed. Doornbos, D.J., Academic Press, New York.

Sieminski, A., Leveque, J.-J. & Debayle, E., 2004. Can finite-frequency effects be accounted for in ray theory surface wave tomography?, *Geophys. Res. Lett.,* **31,** L24614, doi:10.1029/2004GL021402.

Snieder, R., 1986. 3-D linearized scattering of surface waves and a formalism for surface wave holography, *Geophys. J. R. astr. Soc.,* **84,** 581–605.

Spetzler, J., Trampert, J. & Snieder, R., 2002. The effects of scattering in surface wave tomography, *Geophys. J. Int.,* **149,** 755–767.

Tarantola, A. & Valette, B., 1982. Generalized non-linear problems solved using the least-squares criterion, *Rev. Geophys. Sp. Phys.,* **20,** 219–232.

Trampert, J. & Woodhouse, J.H., 1995. Global phase velocity maps of Love and Rayleigh waves between 40 and 150 seconds, *Geophys. J. Int.,* **122,** 675–690.

Trampert, J. & Woodhouse, J.H., 2001. Assessment of global phase velocity models, *Geophys. J. Int.,* **144,** 165–174.

van der Lee, S. & Nolet, G., 1997. Upper mantle S-velocity structure of North America, *J. geophys. Res.,* **102,** 22 815–22 838.

Weeraratne, D.S., Forsyth, D.W., Fischer, K.M. & Nyblade, A.A., 2003. Evidence for an upper mantle plume beneath the Tanzanian craton from Rayleigh wave tomography, *J. geophys. Res.,* **108,** 2427, doi:10.1029/2002JB002273.

Wielandt, E., 1993. Propagation and structural interpretation of non-plane waves, *Geophys. J. Int.,* **113,** 45–53.

Woodhouse, J.H. & Dziewonski, A.M., 1984. Mapping the upper mantle: three-dimensional modeling of earth structure by inversion seismic waveforms, *J. geophys. Res.,* **89,** 5953–5986.

Yang, Y. & Forsyth, D.W., 2006. Rayleigh wave phase velocities, small-scale convection and azimuthal anisotropy beneath southern California, submitted to *J. geophys. Res.,* in press.

Yoshizawa, K. & Kennett, B.L.H., 2002. Determination of the influence zone for surface wave paths, *Geophys. J. Int.,* **149,** 440–453.

Zhou, Y., Dahlen, F.A. & Nolet, G., 2004. 3-D sensitivity kernels for surface-wave observables, *Geophys. J. Int.,* **158,** 142–168.